Front. Phys., 2012, 7(2): 200–207
DOI 10.1007/s11467-011-0204-1

REVIEW ARTICLE

Quantum spin Hall effect in inverted InAs/GaSb quantum wells

Ivan Knez*, **Rui-Rui Du**†

Department of Physics and Astronomy, Rice University, Houston, TX 77251-1892, USA

*E-mail: *ik5@rice.edu, †rrd@rice.edu*

Received May 3, 2011; accepted June 1, 2011

We review the recent experimental progress towards observing quantum spin Hall effect in inverted InAs/GaSb quantum wells (QWs). Low temperature transport measurements in the hybridization gap show bulk conductivity of a non-trivial origin, while the length and width dependence of conductance in this regime show strong evidence for the existence of helical edge modes proposed by Liu *et al.* [Phys. Rev. Lett., 2008, 100: 236601]. Surprisingly, edge modes persist in spite of comparable bulk conduction and show only weak dependence on magnetic field. We elucidate that seeming independence of edge on bulk transport comes due to the disparity in Fermi-wave vectors between the bulk and the edge, leading to a total internal reflection of the edge modes.

Keywords quantum spin Hall effect, InAs/GaSb quantum wells, topological insulators

PACS numbers 73.43.-f, 73.63.Hs, 03.65.Vf

Contents

1 Introduction and background

Recent discovery of topological insulators (TI) has sparked much interest, with flurry of theoretical proposals and intensive efforts on experimental side to observe many of the predicted exotic properties of TIs, from axion dynamics to Majorana fermion excitations [1, 2]. Following the theoretical work of Kane and Mele [3], and independently, Bernevig and Zhang [4], topologically insulating phase, which in two-dimension (2D) is dubbed quantum Spin Hall effect, has been soon experimentally realized in HgTe/CdTe quantum wells [5, 6]. Furthermore, signatures of topologically insulating phase have also been observed in 3D systems of Bi_2Se_3, in ARPES and STM measurements [7–9], albeit hindered in transport experiments by a highly conductive bulk. Thus, from the transport perspective, so far, inverted HgTe/CdTe quantum wells are the only material showing truly insulating bulk and non-local helical edge mode transport – a defining characteristic of TIs. Another well developed semiconducting system which benefits from years of research and shows evidence for existence of QSHI phase are broken type InAs/GaSb quantum wells [10–12]. Compared to HgTe/CdTe, InAs/GaSb carries a series of advantages including continuously tunable band structure via electrical fields [13], as well as a good interface with superconductors [14]. Thus, this material system may prove uniquely suitable for the realization of TI/superconductor hybrid structures [15], which are predicted to host exotic Majorana fermion modes and can be used for topological quantum computation.

InAs, GaSb, and AlSb belong to a class of lattice matched compounds, commonly referred to as the 6.1A family [16], which is the approximate lattice constant of all three materials. In this system, AlSb serves as a good quantum well barrier to narrow gap InAs with a very high band offset of 1.35 eV, enabling deep quantum wells. In addition, small electron effective mass in InAs results in the second highest room temperature mobility of all semiconductors (the first is InSb), making this material very interesting, especially from a device perspective.

Nevertheless, the most attractive aspect of the 6.1A family is its unusual broken gap band alignment between InAs and GaSb, with conduction band of InAs some 150 meV lower than the valence band of GaSb. This allows for coexistence of closely separated electron (in InAs) and

hole (in GaSb) two-dimensional gases that are confined by neighboring AlSb barriers as shown in Fig. 1 [13]. In wider wells, the band structure is inverted with ground conduction sub-band (E1) lower than the ground heavy-hole subband (H1), while the narrower wells have normal progression of states in energy from valence to conduction. In the inverted regime, E1 and H1 bands anti-cross for some wave-vector k_{cross}, where electron and hole densities are approximately matched, $n = p = k_{\mathrm{cross}}^2/2\pi$ and particle energy and in-plane momentum in two wells are equal [13]. Due to the tunneling between the wells, electron and hole states are mixed and a hybridization gap Δ of few meV opens in otherwise semi-metallic band dispersion, as shown in Fig. 1.

Furthermore, transfer of charge between InAs and GaSb layers will result in electric field along the growth axis, which can be tuned via external front and back gates as illustrated in Fig. 1. Changing this built-in field will result in a relative shift of H1 and E1 bands, resulting in a smaller or larger energy separation between the bands, denoted as E_{g0} in Fig. 1. As theoretically shown by Naveh and Laikhtman, even moderate electric fields can drastically change the character of band structure from inverted to normal, and vice versa [13]. In addition, absolute gate bias will determine the position of the Fermi level, and thus, in double-gated configuration both system band structure as well as position of the Fermi level can be tuned with external gates.

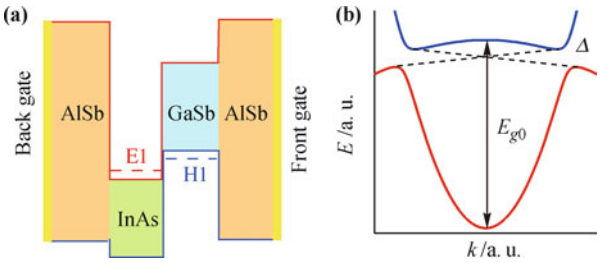

Fig. 1 Band structure and band dispersion of inverted InAs/GaSb QWs.

As mentioned previously, spectrum of the inverted InAs/GaSb QWs, which is shown in Fig. 1, is necessarily gapped. Furthermore, inverted progression of the bands makes this gap topologically distinct from the gap associated with normal progression of bands in normal insulator. Hence, at the edge of the sample, inverted gap must close before the normal insulating gap, such as that in air or omnipresent native oxides, opens, resulting in linearly dispersing edge modes. Time-reversal symmetry considerations require the edge modes to be helical with counter-propagating spin up and spin down channels [10]. Due to the conservation of helicity, particles on time reversed paths around non-magnetic impurity in helical edge destructively interfere, resulting in zero backscattering probability [2]. Thus, in inverted regime of InAs/GaSb, the edge modes are not only guaranteed but also robust against disorder.

Within Landauer–Buttiker formalism, expected edge conductance in six-terminal configuration for mesoscopic samples will be $2e^2/h$ [5], while for four-terminal devices the conductance is doubled to $4e^2/h$. Nevertheless, unlike in quantum Hall systems where edge conductance is present even in macroscopic samples, in quantum spin Hall systems, for longer devices the loss of phase coherence will allow counter-propagating edge modes to backscatter and the conductance will decay with length of the device – illustrating the simple but fundamental difference between one way and two way traffic. Longer samples can be modeled by inserting phase breaking probes and applying Landauer–Buttiker formula obtaining for four terminal devices the following expression [17]:

$$G_{14,23} = \frac{2e^2}{h}\left[\frac{l_\varphi}{L} + \left(\frac{l_\varphi}{L}\right)^2\right]$$

where l_ϕ is the phase coherence length and L is the device length. Thus, for macroscopic QSH samples where $L \gg l_\phi$ edge contribution to conductance will be negligible. As a result, transport in macroscopic samples reflects only the character of the bulk. Earlier transport studies of inverted InAs/GaSb QWs [18, 19], which have been only conducted on larger samples, have confirmed a hybridization gap in the bulk, although all data show a residual conductivity down to the lowest temperatures. Such a lack of true insulating behavior indicates a substantial bulk conduction of intrinsic origin in this material system. We discuss this particular issue in the next section.

2 Bulk conductivity in hybridization gap of inverted InAs/GaSb quantum wells

Mini-gap due to electron-hole hybridization has been first experimentally established in capacitance and transport measurements by Yang *et al.* [18], who have studied front gated InAs/GaSb composite QWs in both inverted and normal regime. Furthermore, evidence for the hybridization gap has been presented in far-infrared measurements of Kono *et al.* [20] and later Yang *et al.* [21]. Similarly, transport experiments by Cooper *et al.* [19] on double gated structures have shown strong resistance peaks, corresponding to the hybridization gap; however, Cooper *et al.* [19] have found that resistance of the mini-gap does not diverge and does not show thermal activation, as may be expected for ideally hybridized system, and have ascribed this oddity to possible band anisotropy and impurity states within the mini-gap. In fact, in the earliest study, it has been found by Yang *et* al. [18] that the capacitance signal, which corresponds directly to density of the states, exhibits only slight dip in hybridization gap, compared to large reduction of density of states in the normal gap, presumably due to localized states present in

hybridization gap and curiously absent in normal gap of similar size. Note that these early studies have all been performed on macroscopic samples, and as previously suggested, possible edge contributions to the observed finite gap conductivity in these studies can be safely excluded.

The issue of residual bulk conductivity has been theoretically resolved by Naveh and Laikhtman [22], who considered tunneling between the wells to be dissipative, albeit slightly. In early theoretical studies, Caldeira and Legett [23] have found that dissipation, i.e., coupling of the quantum mechanical particle to external degrees of freedom, will lead to reduced quantum mechanical capacity of the particle for tunneling. Thus, dissipative tunneling will leave some proportion of electronic states non-hybridized, giving non-zero density of states in the gap and finite gap conductivity. Using the full quantum approach of Keldysh formalism, Naveh and Laikhtman have shown that a slight amount of electron and hole level broadening leads to drastic changes in transport behavior, giving finite bulk conductivity even at zero temperature and even in the limit when level broadening is much smaller than the size of the mini-gap [22]. In fact, in the limit of small level broadening Γ and for small Δ, such that $\Gamma \ll \Delta \ll E_{g0}$, zero-temperature bulk conductivity approximately scales as [22]:

$$g(T=0) \propto \frac{e^2}{h}\frac{E_{g0}}{\Delta}$$

Thus, for negligible level broadening the gap conductivity depends only on band parameters. This is due to the fact that level broadening gives free charge carriers in the gap whose number goes as Γ and whose mobility scales as $1/\Gamma$ resulting in finite conductivity independent of broadening.

The latter surprising result has been confirmed in our recent experimental study [11], which showed the bulk conductivity on the order of $\gtrsim 10e^2/h$ and few times larger than the expected contribution from the edge. Our high quality wafers were grown by molecular beam epitaxy on silicon-doped $N^+(100)$ GaAs substrate, which serves as a back gate. The structure consists of a standard buffer consisting of AlSb and $Al_{0.8}Ga_{0.2}Sb$ layers which accommodates for about 7% lattice mismatch between GaAs and AlSb [24]. On top of this a 500 Å AlSb lower barrier was grown, followed by 150 Å InAs and 80Å GaSb quantum wells with a 500Å AlSb top barrier and 30 Å GaSb cap layer to prevent from oxidation of the AlSb barrier. Under zero applied bias only electrons are present in the well, with a typical low temperature density of $7\times10^{11}\mathrm{cm}^{-2}$ and mobility of approximately 10^5 $\mathrm{cm}^2/\mathrm{Vs}$.

Samples are processed using standard photo- and e-beam lithography techniques with wet etching. The top gate was fabricated by depositing Si_3N_4 using plasma enhanced chemical vapor deposition system, and evaporating metal gates. Low temperature magneto-transport measurements were carried out in a ^{3}He refrigerator (300 mK) combined with a 12 T superconducting magnet, or in a ^{3}He/^{4}He dilution refrigerator (20 mK) with a 18 T magnet (National High Magnetic Field Laboratory). Standard lock-in technique with an excitation current of 100 nA at 23 Hz was employed.

Figure 2(a) shows longitudinal resistance R_{xx} vs. front gate bias V_{front} of a 0.7 μm by 1.5 μm six-terminal Hall bar structure, at temperatures from 0.3 K to 40 K in approximately 2K steps. When the Fermi level is pushed into the hybridization gap clear peaks in resistance are observed. Resistance peaks do not show thermal activation, although they persist to temperatures up to 30–40 K, suggesting that the size of hybridization gap is approximately 3–4 meV, which is consistent with previously reported values. Note that the maximum resistance observed is on the order of 4 kΩ, and is few times smaller than the contribution from proposed edge modes of $h/(2e^2)$ ~12.9 kΩ, indicating dominant bulk transport in these structures.

Furthermore, by adjusting the back gate bias, relative separation between the bands E_{g0} can be reduced, resulting in an approximately linear decrease of bulk conductivity with anti-crossing density, $n = p = E_{g0}\frac{m^*}{\pi\hbar^2}$, and is shown in Fig. 2(b), where m^* is the reduced mass, $m^* = \frac{m_e \cdot m_h}{m_e + m_h}$, with carrier masses m_e =0.03 and m_h=0.37 (in units of free electron mass) [18]. This is in reasonable agreement with the crude estimate of bulk conductivity given by Naveh and Laikhtman [22], with both experimental values and theoretical estimates shown in Fig. 2(b) for Δ=3.6 meV. Discrepancy at larger densities is presumably due to band anisotropy, which for simplicity has been ignored in their theory.

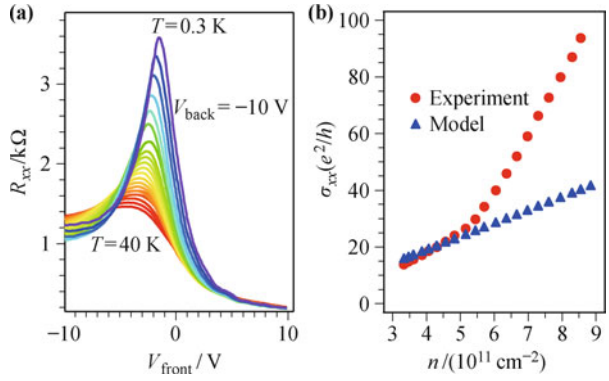

Fig. 2 Panel **(a)** shows resistance peaks for temperatures from 0.3 K to 40 K in roughly 2K steps. Resistance peaks lack thermal activation but persist up to 30–40 K, suggesting Δ~3–4 meV. Panel **(b)** shows bulk conductivity vs. anti-crossing density for both experiment and theory, giving good agreement at lower densities where band anisotropy can be ignored.

In addition, at lower anti-crossing densities where band anisotropy is strongly reduced, besides resistance peaks we also observe resistance dips shown in Fig. 3.

These dips correspond to van Hove singularities in density of states (DOS) at the edges of the gap [18], as illustrated in the same figure. From the relative position of resistance dips and peaks [Fig. 3(a), (b)] in front gate bias as we can estimate mini-gap value $\Delta \approx 2\,(V_{\rm peak} - V_{\rm dip})\,\frac{\Delta n}{\Delta V}\frac{1}{DOS}$, where $\frac{\Delta n}{\Delta V}$ is the rate of carrier density change with front bias, and $DOS = \frac{m_e + m_h}{\pi\hbar^2}$, obtaining Δ=3.6 meV. Note that applying the in-plane field shifts electron and hole bands in opposite directions, inducing the band anisotropy and weakening the dips as shown in Figs. 3(c) and (d).

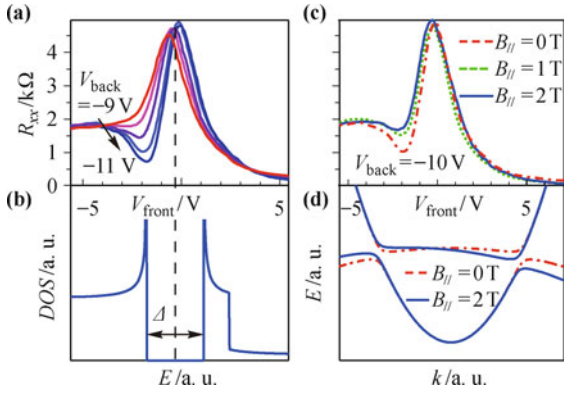

Fig. 3 Panel **(a)** evolution of resistance dips as the $V_{\rm back}$ is varied from −9 V to −11 V, in 0.5 V steps, B =0 T, T =20 mK. Resistance dips occur at singularities in DOS near gap edges shown in **(b)**. From relative position of dips and peaks in $V_{\rm front}$ we determine $\Delta \approx 3.6$ meV. Dips weaken with in-plane magnetic field in **(c)**, due to induced anisotropy in the dispersion in **(d)**. Reproduced from Ref. [11], Copyright © 2010 American Physical Society.

In conclusion, in inverted InAs/GaSb quantum wells disorder has a singular effect, resulting in finite bulk conductivity even in the limit of relatively small level broadening of electron and hole levels, as revealed by theoretical work of Naveh and Laikhtman, and confirmed by our experiments. Thus, the residual bulk conductivity is not a simple dirt effect, which can be removed by improving the cleanliness of the system, but a subtle yet profound consequence of dissipative quantum tunneling in realistic electron–hole systems. Nevertheless, this result suggests that bulk conductivity can be substantially reduced as the band-structure is tuned towards a critical point by decreasing the relative separation between the bands E_{g0}, thus potentially opening a viable regime for observing quantum spin Hall insulating phase. In the next section, we look in exactly such a parameter regime, where the bulk conductivity is reduced, and by studying the length and width dependence of the mini-gap conductance we find the evidence for helical edge modes.

3 Length and width dependence of conductance in hybridization regime – Evidence for helical edge modes

Motivated by the latter results, we have reduced the size of the quantum wells to 125 Å InAs and 50 Å GaSb, resulting in the reduced bulk conductivity by a factor of 2–3, but similar quantum well quality, i.e., comparable zero gate bias mobility [12]. Furthermore, in order to increase the relative edge contribution we study four terminal structures, and in this case the expected bulk contribution will be comparable to or smaller than the helical edge conductance of $4e^2/h$. For a macroscopic sample with the length L =100 μm and a geometric factor $\gamma = L/W = 2$, resistance peaks in these narrower wells increase to $R_{\rm max}$∼10.2 kΩ as shown in Fig. 4, when the Fermi level is tuned through the hybridization gap. Note that in such a long sample, the edge contribution is negligible and the observed resistance value reflects only the bulk transport, with the bulk conductivity of $g_{\rm measured} = \gamma/R_{\rm max} = 5.05e^2/h$.

The entry into hybridization gap is also signaled by non-linearity in $B/(eR_{xy})$ (in blue and taken at B = 1 T), which in a linear regime corresponds to the electron density. The negative values of $B/(eR_{xy})$ indicate a hole dominated regime although in a two-carrier regime the direct correspondence to the carrier density no longer exists. As discussed previously, the size of the mini-gap can be determined from the relative position in gate bias of resistance dip obtaining Δ ∼4 meV.

Relative separation between electron and hole bands is estimated from the minimum in $B/(eR_{xy})$, which corresponds to the anti-crossing density $n_{\rm cross} \sim 2{\times}10^{11}$ cm^{-2}, giving $E_{g0} = \frac{n_{\rm cross}\pi\hbar^2}{m^*} \approx 16$ meV. Thus, the theoretical estimate of the bulk conductivity from band parameters and using Eq. (2) is $g_{\rm expected}$ ∼4e$^2/h$, which is in close agreement with the resistance peak value shown in Fig. 4.

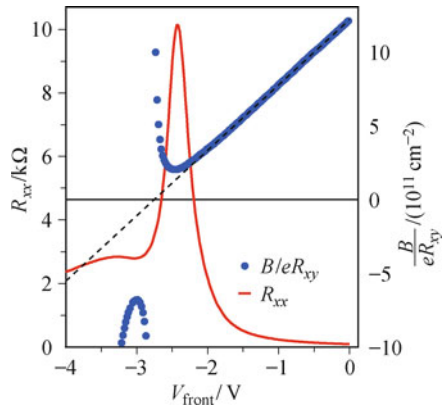

Fig. 4 Longitudinal resistance (in red) and $B/(eR_{xy})$ (in blue), taken at B = 1 T, vs. front gate bias $V_{\rm front}$ of a 50 μm by 100 μm long Hall bar at B = 0 T. As the $V_{\rm front}$ is swept from 0 V to −4 V, Fermi level is pushed from purely electron to two-carrier hole dominated regime. Strong resistance peak of $R_{\rm max}$∼10.2 kΩ occurs when electron and hole densities are matched. Reproduced from Ref. [12], Copyright © 2011 American Physical Society.

Next we reduce the length of devices from L = 100 μm down to 10 μm, 4 μm, and 2 μm, while varying the width to keep the constant geometric factor γ = 2.

As the length of the device is reduced from macroscopic to mesoscopic dimensions, the value of the resistance peaks decreases sharply as shown in Fig. 5(a). Furthermore, note that the edge contribution in the macroscopic 100 μm long sample is negligible, and the resistance peak of this device can be used to estimate the gap resistance of the bulk $R_{\rm bulk}$∼10.2 kΩ. The parallel combination of $R_{\rm bulk}$ and the expected helical edge resistance of $h/(4e^2)$ gives the resistance value of $R_{\rm bulk}\|h/(4e^2)$∼3.95 kΩ, which is only slightly above the measured resistance peak value of the mesoscopic 2 μm long sample, where $R_{\rm max}$ ∼3.75 kΩ, confirming the helical edge picture.

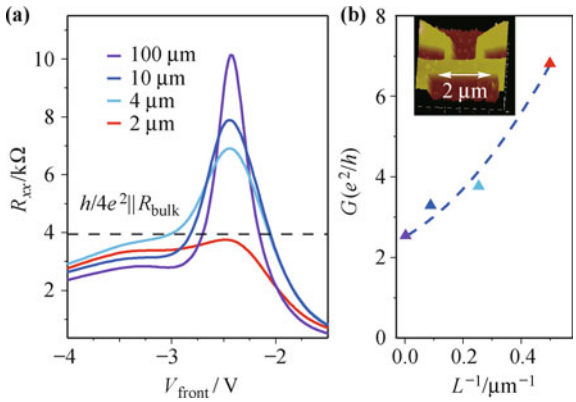

Fig. 5 Panel **(a)** shows R_{xx} vs. $V_{\rm front}$ for devices with L = 100 μm, 10 μm, 4 μm, and 2 μm (AFM image in inset of panel (b), with constant geometric factor $\gamma = 2$. Panel **(b)** shows gap conductance G vs. L^{-1}. Reproduced from Ref. [12], Copyright © 2011 American Physical Society.

Similarly, gap conductance G plotted vs. inverse device length $1/L$ in Fig. 5(b) shows strong decrease with length, with a difference in conductance between smallest and largest samples slightly larger than $4e^2/h$, which is indicative of helical edge mode transport. Note that the bulk conductivity also scales with the length. However, this logarithmic correction [25] to bulk conductance can be estimated as $\Delta G \approx \frac{e^2}{\gamma\pi h} Ln\left(\frac{100\ \mu m}{2\ \mu m}\right) \approx 0.6\frac{e^2}{h}$, and thus accounts for only a fraction of the total observed differences in conductance between mesoscopic and macroscopic samples. In addition, gap conductance G vs. $1/L$ shown in Fig. 5(b) can be fitted reasonably well with Eq. (1), obtaining the coherence length value l_ϕ ∼2 μm. Thus, compared to macroscopic samples, the mesoscopic samples show additional conductance of approximately $4e^2/h$, presumably from helical edge modes. Besides, the gap conductance shows a length dependence trend that is in close agreement with what is expected for helical edge modes.

Additional evidence for edge modes is found in the width dependence of gap resistance in mesoscopic samples. Figure 6(a) shows resistance peaks of four devices of equal length L = 2 μm, but with different width, W = 0.5 μm, 1 μm, 1.5 μm, to 2 μm. In this case, resistance peaks decrease as the device width is reduced, as expected for bulk transport; however, the gap conductance showing linear dependence on W, has a non-zero intercept of linear fit, which is in sharp contrast to the solely bulk conduction. In fact, the intercept value of $G_{\rm edge}$∼ $4e^2/h$ strongly suggests the existence of helical edge conduction channels. As an important check, the slope of the linear fit to G vs. W trace gives the bulk conductivity $g = (5.46\pm1.01)\ e^2/h$, which is consistent with the previously determined values. In conclusion, both the length and width dependence of the gap resistance and conductance indicate the existence of helical edge channels in inverted InAs/GaSb quantum wells.

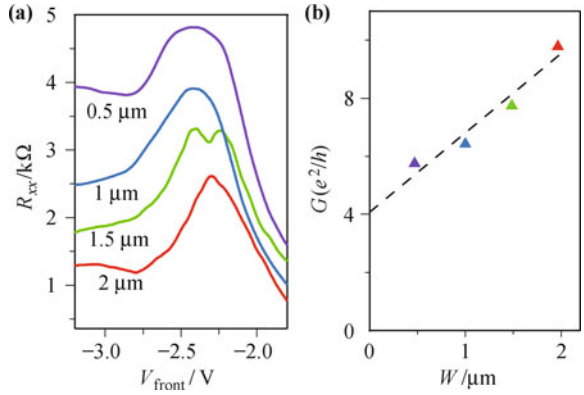

Fig. 6 Panel **(a)** shows R_{xx} vs. $V_{\rm front}$ for devices with L = 2 μm, and W = 0.5 μm, 1 μm, 1.5 μm, to 2 μm. Resistance peaks decrease as W is increased. In **(b)** G vs. W shows linear relationship with intercept of $4e^2/h$ consistent with helical edge modes. Reproduced from Ref. [12], Copyright © 2011 American Physical Society.

Furthermore, using the back gate bias we can tune the anti-crossing point to lower wave-vector values. Figure 7 shows R_{xx} vs. $V_{\rm front}$ with $V_{\rm back}$ varied in 2 V steps from 0 V to −8 V for devices of L =100 μm in (a) and L = 2 μm in (b), $\gamma = 2$ in both cases. As $V_{\rm back}$ is tuned to more negative values, the separation between the bands E_{g0} is reduced, and the resistance peaks of 100 μm long sample increase from $R_{\rm max}$ ∼ 10 kΩ at $V_{\rm back}$ =0 V to $R_{\rm max}$ ∼ 50 kΩ at $V_{\rm back}$ = −8 V. On the other hand, the resistance peaks of the mesoscopic sample increase only slightly, from about $R_{\rm max}$ ∼ 4 kΩ at $V_{\rm back}$ =0V, to $R_{\rm max}$ ∼ 6 kΩ at $V_{\rm back}$ = −8V. In fact, difference in conductance between macroscopic and mesoscopic samples $\Delta G = G_{2\mu m} - G_{100\mu m}$ stays around $4e^2/h$ for all values of back gate bias, as shown in the inset of Fig. 7, giving further evidence for helical edge modes. We mention here in passing that resistance peaks shift towards more positive $V_{\rm front}$ as $V_{\rm back}$ is made more negative, which is due to the fact that resistance peaks occur at the charge neutral point, and hence $\Delta Q = 0$. As a result, from the simplest capacitance considerations we have $\Delta V_{\rm back} \cdot C_{\rm back} + \Delta V_{\rm front} \cdot C_{\rm front} = 0$, where $C_{\rm back}$ and $C_{\rm front}$ are capacitances of front and back gates.

The data presented in Fig. 7 may suggest that edge conduction is completely independent of bulk conduc-

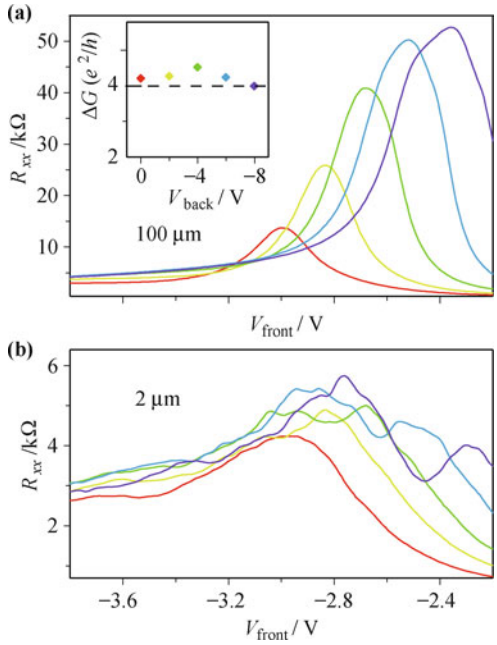

Fig. 7 The figure shows R_{xx} vs. $V_{\rm front}$ for devices with L =100 μm in **(a)** and L =2 μm in **(b)**, with γ= 2 in both cases, with $V_{\rm back}$ varied in 2 V steps from 0 V to −8 V. Inset shows difference in conductance between macroscopic and mesoscopic samples, $\Delta G = G_{2\mu\rm m} - G_{100\mu\rm m}$ vs. $V_{\rm back}$, which stays around $4e^2/h$ for all values of back gate bias. Reproduced from Ref. [12], Copyright © 2011 American Physical Society.

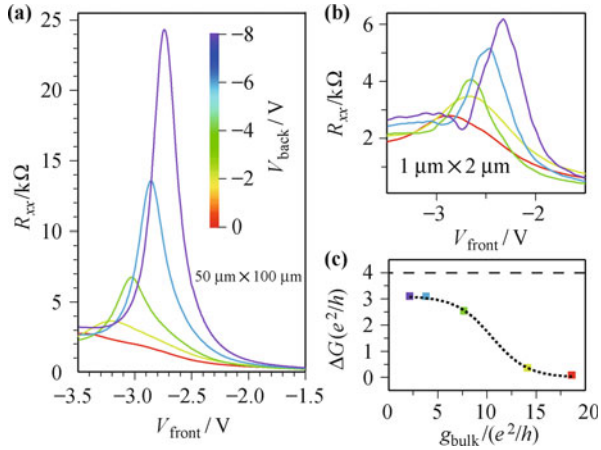

Fig. 8 The figure shows R_{xx} vs. $V_{\rm front}$ for bias cooled devices with L =100 μm in **(a)** and L =2 μm in **(b)**, with γ =2 in both cases, with $V_{\rm back}$ varied in 2V steps from 0 V to −8 V. Panel **(c)** shows $\Delta G = G_{2\mu\rm m} - G_{100\mu\rm m}$ vs. bulk conductivity $g_{\rm bulk}$. Edge conduction "activates" for $g_{\rm bulk} < 10e^2/h$. Reproduced from Ref. [12], Copyright © 2011 American Physical Society.

tivity. However, this is valid only in the limit of low bulk conductivity. Note that in Fig. 7, the gap bulk conductivity is varied from about $g \sim 5e^2/h$ at $V_{\rm back}$ =0V, to $g \sim 0.5e^2/h$ at $V_{\rm back} = -8$ V. Using bias cooling technique [11], it is possible to shift the starting point deeper into the inverted regime, i.e., a larger E_{g0} can be obtained, so that at $V_{\rm back}$ =0V, $g \sim 19e^2/h$, while at $V_{\rm back} = -8$ V, $g \sim e^2/h$, as shown in Fig. 8. In this case, the edge conductance, i.e., $\Delta G = G_{2\mu\rm m} - G_{100\mu\rm m}$, goes from $\Delta G \sim 0$ for large bulk conductivity of $g \sim 19e^2/h$ to about $\Delta G \sim 3e^2/h$ as the bulk conductivity is reduced to $g < 5e^2/h$. In fact, the cut-off bulk conductivity at which the edge conduction "activates" can be estimated to $g \sim 10e^2/h$.

Apparent indifference of edge conduction to bulk transport, at least for smaller values of bulk conductivity, which is evident in Figs. 7 and 8, is quite surprising considering that the conductive bulk would provide scattering channels for the edge modes situated on the opposite sides of the device, and hence the edge conductance would diminish [26, 27]. In a recent theoretical study of QSH edges in quantum point contact geometry where tunneling between edge modes on opposite sides is enabled by reducing the device width, it has been found that the decrease in two-terminal helical edge conductance is roughly proportional to $T\sin^2\theta$, where θ is the angle between the spin direction and the growth axis, and T is the tunneling probability [27]. Thus, even for a large tunneling probability, the edge conductance will not diminish if the spins are oriented normal to the quantum well plane, which is the case for the weak Rashba spin orbital interaction.

Furthermore, the tunneling probability between opposite side edges may be significantly reduced by large Fermi wave-vector mismatch. Note that the bulk gap states are inherited from non-hybridized band structure and generally will have Fermi wave-vector equal to $k_{\rm cross}$ while edge modes for Fermi energy situated in the middle of the gap have a wave-vector close to zero. Thus, for larger $k_{\rm cross}$, the edge modes will be totally reflected from the bulk states. In fact, the tunneling probability for the edge electron will be proportional to the edge-bulk transmission probability, which can be expected to go as $k_{\rm edge}/k_{\rm cross}$ and bulk transmission, which scales as bulk conductivity, i.e., as $E_{g0} \sim k^2_{\rm cross}$. Hence, it follows that the tunneling probability will decrease as $k_{\rm cross}$ is reduced. This picture qualitatively agrees with data presented in Fig. 8, where edge conduction activates for smaller bulk conductivity, i.e., the regime of reduced E_{g0} and $k_{\rm cross}$, and hence closer to the critical point. Nevertheless, a full quantum theoretical treatment of the problem, which would include the dissipation into tunneling between the wells, similar to Ref. [28], is hoped to reveal more details regarding the stark resilience of edge transport to conductive bulk.

Next we turn to magnetic field dependence of gap transport in mesoscopic and macroscopic samples. Surprisingly, the resistance peaks of mesoscopic samples show only weak dependence on in-plane and perpendicular magnetic fields as shown in Figs. 9(a) and (b), while macroscopic samples show much stronger dependence. At first glance, this appears to be in contrast to the strong field dependence observed in HgTe/CdTe quantum wells [5] and the notion of time reversal break-

ing, which spoils the perfect destructive interference of backscattering paths and leads to a fast decay of edge conductance in the perpendicular field.

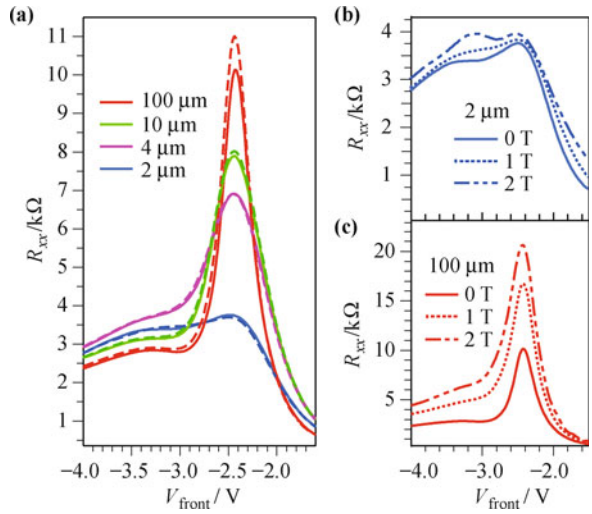

Fig. 9 Panel **(a)** shows R_{xx} vs. V_{front} at $B_{//}$=0T (*full line*) $B_{//}$=1 T (*dashed*) for L =100 μm, 10 μm, 4 μm, and 2 μm devices, indicating weak field dependence of gap resistance. Panel **(b)** shows R_{xx} vs. V_{front} at B_{perpend}=0 T, 1 T, and 2 T for L =2 μm; and in panel **(c)** for L =100 μm. Reproduced from Ref. [12], Copyright © 2011 American Physical Society.

However, we note here that even in HgTe the strong magnetic field dependence has never been observed in the smallest micron size samples, but in longer 20 μm long samples [5, 29]. In fact, it has been shown theoretically by Maciejko *et al.* [28], using the full quantum approach of Keldysh formalism, that magnetic field decay of edge modes depends sensitively on the disorder strength, with pronounced cusp like features of conductance in the magnetic field occurring only when the disorder strength is larger than the size of the gap. The interpretation of this result was that by providing the states in the bulk by a large disorder, edge electrons can diffuse into a bulk enclosing larger amounts of flux whose accumulation destroys destructive interference of backscattering paths, resulting in a linear decay of conductance with B. In the case of HgTe, a large disorder was provided by inhomogenous gating, which is more pronounced for longer devices.

Naively, it appears that the edge modes in InAs/GaSb should have very strong field dependence due to the strong bulk conduction. However, due to the Fermi wave-vector mismatch between the edge and bulk that we previously discussed, the edge states are presumably totally reflected from the bulk. Note that this happens even for a larger disorder, simply due to the fact that unlike in HgTe where the gap opens at k =0, in InAs/GaSb the gap opens at k values, generally much larger than zero, and hence in the middle of the gap, the bulk states will necessarily have Fermi wave-vectors significantly larger than the edge. Thus, due to this decoupling of edge from bulk, the magnetic field dependence of edge modes is expected to be weak.

On the other hand, decay of the bulk conductivity with magnetic field may not necessarily be weak due to the localization of non-hybridized carriers which contribute to non-zero bulk conductivity in the first place. However, this localization is more pronounced for longer samples where disorder is naturally stronger. Thus, similarly to HgTe, but for different physical reasons, i.e., not due to the decay of edge conductance with B but due to the decay of bulk conductivity, longer samples are expected to show stronger magnetic field dependence, as observed. At any rate, due to the gap opening far from the zone center, the edge modes in InAs/GaSb are qualitatively different from those in HgTe/CdTe where the gap opens at the zone center, showing striking resilience to both bulk conduction as well as applied magnetic fields.

Finally, we note here that the topologically non-trivial band-structure in InAs/GaSb is also evidenced at high magnetic fields, showing peculiar re-entrant quantum Hall behavior [30, 31]. Such re-entrant quantum Hall behavior has also been observed in HgTe [5], where the system switches from insulating to integer quantum Hall regime at ν=1 and back to insulating at higher fields, and has been taken as a direct evidence of topologically non-trivial gap. In InAs/GaSb the origin of such peculiar magnetic field behavior is its non-monotonic band structure. Under a perpendicular magnetic field the continuous density of states separates into a series of discrete Landau levels whose dispersion in the magnetic field can be obtained from the zero-field by transforming $k \propto \sqrt{B}$ [13]. In consequence, non-monotonic zero field spectrum will give similarly non-monotonic Landau level spectrum. At the field values which correspond to anti-crossing wave-vector and band extrema, LL spectrum is gapped and the system switches to an insulating regime. Further away from the band extrema, the system exhibits normal quantum Hall behavior. Such re-entrant quantum Hall behavior is a signature mark of topologically distinct band structure and, as theoretically argued [1,10], guarantees the edge modes at a zero field.

4 Conclusions and future directions

Finally, InAs/GaSb exhibits transport properties characteristic of quantum spin Hall systems, with a band structure whose inverted character is signaled by re-entrant quantum Hall behavior, and with apparent edge conduction channels which persist despite conductive bulk and show only weak magnetic field dependence. We have argued that this unusual behavior can be qualitatively explained by the fact that in this system the inverted gap opens away from Brillouin zone center, unlike in HgTe. In consequence, hybridization gap, which has long been

experimentally established, exhibits non-zero bulk conductivity. Thus, non-zero bulk conductivity arises due to finite level broadening of electron–hole levels and non-zero anti-crossing wave-vector between the electron hole bands.

Despite this conductive bulk, the length and width dependence of transport coefficients in InAs/GaSb QWs in inverted regime suggest the existence of helical edge modes, which show only weak dependence on magnetic fields. This is again due to the gap opening far from the zone center, which results in relative decoupling of edge channels to bulk states due to large disparity in Fermi wave-vectors, giving strong resilience of edge modes to conductive bulk and applied magnetic fields. Similar to HgTe, a separate evidence for topological band structure can be found at high magnetic fields. In this case, band hybridization results in non-monotonic LLs and non-trivial magnetic properties with re-entrant Quantum Hall behavior. Demonstrated band structure tunability and good interface to superconductors make this quantum spin Hall system a promising candidate in realization of exotic Majorana modes.

Acknowledgements The work at Rice was supported by Rice Faculty Initiative Fund, Hackerman Advanced Research Program grant 003604-0062-2009, Welch Foundation grant C-1682, and NSF grant DMR-0706634. I.K. acknowledges partial support from M. W. Keck Scholar. We thank S.-C. Zhang for bringing our attention to Ref. [10], S.-C. Zhang, X.-L. Qi, C. Liu, J. Maciejko, and M. Konig for many helpful discussions.

References

1. M. Z. Hasan and C. L. Kane, Rev. Mod. Phys., 2010, 82: 3045
2. X. L. Qi and S.C. Zhang, arXiv:1008.2026, 2010
3. C. L. Kane and E. J. Mele, Phys. Rev. Lett., 2005, 95: 226801
4. B. A. Bernevig and S. C. Zhang, Phys. Rev. Lett., 2006, 96: 106802
5. B. A. Bernevig, T. L. Hughes, and S. C. Zhang, Science, 2006, 314: 1757
6. M. König, S. Wiedmann, C. Brüne, A. Roth, H. Buhmann, L. W. Molenkamp, X. L. Qi, and S. C. Zhang, Science, 2007, 318: 766
7. D. Hsieh, D. Qian, L. Wray, Y. Xia, Y. S. Hor, R. J. Cava, and M. Z. Hasan, Nature, 2008, 452: 970
8. P. Roushan J Seo C. V. Parker, Y. S. Hor, D. Hsieh, D. Qian, A. Richardella, M. Z. Hasan1, R. J. Cava, and A. Yazdani, Nature, 2009, 460: 1106
9. P. Cheng, C. Song, T. Zhang, Y. Zhang, Y. Wang, J. F. Jia, J. Wang, Y. Wang, B. F. Zhu, X. Chen, X. C. Ma, K. He, L. Wang, X. Dai, Z. Fang, X. C. Xie, X. L. Qi, C. X. Liu, S. C. Zhang, and Q. K. Xue, Phys. Rev. Lett., 2010, 105: 076801
10. C. Liu, T. L. Hughes, X. L. Qi, K. Wang, and S. C. Zhang, Phys. Rev. Lett., 2008, 100: 236601
11. I. Knez, R. R. Du, and G. Sullivan, Phys. Rev. B, 2010, 81: 201301(R)
12. I. Knez, R. R. Du, and G. Sullivan, Phys. Rev. Lett., 2011, 107: 136603
13. I. Y. Naveh and B. Laikhtman, Appl. Phys. Lett., 1995, 66: 1980
14. C. Nguyen, J. Werking, H. Kroemer, and E. L. Hu, Appl. Phys. Lett., 1990, 57: 87
15. L. Fu and C. L. Kane, Phys. Rev. Lett., 2008, 100: 096407
16. H. Kroemer, Physica E, 2004, 20: 196
17. See: e.g., S. Datta, Electronic Transport in Mesoscopic Systems, Cambridge: Cambridge University Press, 1995
18. M. Yang, C. Yang, B. Bennett, and B. Shanabrook, Phys. Rev. Lett., 1997, 78: 4613
19. L. Cooper, N. Patel, V. Drouot, E. Linfield, D. Ritchie, and M. Pepper, Phys. Rev. B, 1998, 57: 11915
20. J. Kono, B. D. McCombe, I. Lo, W. C. Mitchel, and C. E. Stutz, Phys. Rev. B, 1997, 55: 1617
21. M. J. Yang, C. H. Yang, and B. R. Bennett, Phys. Rev. B, 1999, 60: R13958
22. Y. Naveh and B. Laikhtman, Europhys. Lett., 2001, 55: 545
23. A. Caldeira and A. J. Legett, Phys. Rev. Lett., 1981, 46: 211
24. C. Nguyen, B. Brar, C. R. Bolognesi, J. J. Pekarik, H. Kroemer, and J. H. English, J. Electron. Mater., 1993, 22: 255
25. E. Abrahams, P. W. Anderson, D. C. Licciardello, and T. V. Ramakrishnan, Phys. Rev. Lett., 1979, 42: 673
26. B. Zhou, H. Z. Lu, R. L. Chu, S. Q. Shen, and Q. Niu, Phys. Rev. Lett., 2008, 101: 246807
27. J. I. Väyrynen and T. Ojanen, Phys. Rev. Lett., 2011, 106: 076803
28. J. Maciejko, X. L. Qi, and S. C. Zhang, Phys. Rev. B, 2010, 82: 155310
29. M. Konig, Ph. D. Thesis, Wurzburg University, 2007, private communications
30. R. J. Nicholas, K. Takashina, M. Lakrimi, B. Kardynal, S. Khym, N. J. Mason, D. M. Symons, D. K. Maude, and J. C. Portal, Phys. Rev. Lett., 2000, 85: 2364
31. I. Knez, R. R. Du, and G. Sullivan, to be published